geosciences

MDPI

Article

Depositional Setting, Diagenetic Processes, and Pressure Solution-Assisted Compaction of Mesozoic Platform Carbonates, Southern Apennines, Italy

Simona Todaro [1,*], Canio Manniello [2,3], Alessia Pietragalla [2], Nereo Preto [4] and Fabrizio Agosta [2,3]

[1] Department of Earth and Marine Sciences, University of Palermo, 90123 Palermo, Italy
[2] Department of Sciences, University of Basilicata, 85100 Potenza, Italy; c.manniello@unibas.it (C.M.); alessia.pietragalla@edu.unifi.it (A.P.); fabrizio.agosta@unibas.it (F.A.)
[3] Reservoir Characterization Project, Department of Sciences, University of Basilicata, 85100 Potenza, Italy
[4] Department of Geosciences, University of Padova, 35122 Padova, Italy; nereo.preto@unipd.it
* Correspondence: simona.todaro@unipa.it

Abstract: Pressure solution processes taking place during diagenesis deeply modify the hydraulic properties of carbonates, affecting their mechanical layering and hence the dimension, distribution, and connectivity of high-angle fractures. The formation of stylolites is controlled by the texture of the host rock and therefore by the depositional environment and the diagenetic processes that involve it. This study reports the results of a multidisciplinary study carried out on a Jurassic–Cretaceous carbonate platform in southern Italy. The goal is to unravel the control exerted by single carbonate textures and specific diagenetic processes on the formation of bed-parallel stylolites. Microfacies analyses of thin sections are aimed at obtaining information regarding the composition and texture of the carbonates. Petrographic observations coupled with CL analyses are key to deciphering their diagenetic history. Results are consistent with carbonates originally deposited in a shallow-water realm in which carbonate mud is occasionally abundant. In this environment, early cementation inhibits their chemical compaction. In grain-supported facies, pressure solution is only localized at the grain contacts. During shallow burial diagenesis, precipitation of blocky calcite predates the formation of bed-parallel stylolites in the grain-supported facies. Contrarily, mud-supported facies favor chemical compaction, which results in stylolites showing a good lateral extension and thick sediment infill. A classification of different types of stylolite morphology is attempted in relation to facies texture. In detail, rougher morphology (sharp-peak) characterizes the stylolites nucleated in grain-supported facies, while smoother morphology (rectangular to wave-like) is observed in stylolites on mud-supported facies. Application of this knowledge can be helpful in constraining the diagenetic history of carbonate rocks cored from depth, and therefore predict the fracture stratigraphy properties of carbonates buried at depth.

Keywords: shallow-water limestone; marine platform deposition; microfacies analysis; diagenetic processes; chemical compaction; carbonate reservoir; stylolites

check for updates

Citation: Todaro, S.; Manniello, C.; Pietragalla, A.; Preto, N.; Agosta, F. Depositional Setting, Diagenetic Processes, and Pressure Solution-Assisted Compaction of Mesozoic Platform Carbonates, Southern Apennines, Italy. *Geosciences* **2024**, *14*, 89. https://doi.org/10.3390/geosciences14040089

Academic Editors: Cameron J. Manche, Georgina Lukoczki, Michele Morsilli and Jesus Martinez-Frias

Received: 21 February 2024
Revised: 15 March 2024
Accepted: 16 March 2024
Published: 22 March 2024

Copyright: © 2024 by the authors. Licensee MDPI, Basel, Switzerland. This article is an open access article distributed under the terms and conditions of the Creative Commons Attribution (CC BY) license (https://creativecommons.org/licenses/by/4.0/).

1. Introduction

Within shallow-water carbonates, diagenetic processes such as physical and chemical compaction, cement precipitation, and microfracturing have a profound effect on their composition, texture, porosity, and overall petrophysical properties [1–5]. Focusing on chemical compaction, according to the classification of pressure solution features first proposed by Choquette and Pray [6], two main types of stylolites and pressure solution seams can be distinguished, e.g., (i) non-sutured solution surfaces, which can occur either as single seams or as swarms and often form within carbonates that include a significant content of insoluble material such as clay, silt, and/or organic matter; (ii) sutured solution

surfaces, which correspond to stylolites and grain contact sutures and often form within carbonates with a low content of insoluble residual material.

In terms of the most diffuse structural elements within shallow-water carbonates, bed-parallel stylolites and pressure solution seams are the most common [1,7–19]. These elements cause lithological compaction, volume loss, and bed amalgamation, and might extend for great distances within single carbonate beds and units [10,11,13]. The stylolites can occur as single elements and/or as forming networks. In both cases, they often include insoluble material, and are therefore interpreted as being responsible for porosity and permeability reduction in shallow-water limestones. In particular, recent studies outlined the profound control exerted by bed-parallel solution surfaces in the permeability anisotropy that characterizes shallow-water carbonates [8,10,18,20–23]. Results also showed that pressure solutions associated with chemical compaction are facies-dependent, so that both nucleation and development of stylolites and pressure solution seams have a tight relation with the rock texture [10,14,16,19].

In this work, we aim to identify and characterize the depositional and diagenetic processes occurring in shallow-water carbonates. Together with the time–space assessment of the structural processes, this analysis is key to fully assessing the storage and migration properties of shallow-water carbonates, with implications for fossil and renewable energy production, management of groundwater resources, and carbon capture and storage (CCS) applications [24,25]. Starting from the above consideration, we present the results of an integrated sedimentological, petrographic, and diagenetic study carried out in Lower Jurassic to Cretaceous shallow-water carbonates outcropping along the axial zone of the southern Apennines fold-and-thrust belt, Italy. In detail, we investigate beautiful outcrops exposed along the flanks and at the top of Viggiano Mt., which flanks the intermontane Agri Valley eastward [26–29].

The studied Mesozoic shallow-water carbonates were recently analyzed in terms of their fracture stratigraphy properties [30], modalities of pressure solution processes associated with sedimentary burial- and thrusting-related stress conditions [19], multiscale fault and fracture geometry and distribution [31], and multiscale fracture porosity and permeability characteristics. Focusing on the diagenetic processes during the sedimentary burial (sensu [19]), we first decipher the relative timing of precipitation of the calcite cements in the various carbonate lithofacies, we assess the diagenetic environments in which they formed, and then we document the crosscutting relationships between bed-parallel stylolites and cements. Specifically, regarding the bed-parallel stylolites, [19] documented multiple generations of structures, associated with either sedimentary burial and tectonic burial, due to the Miocene–Pliocene buildup of the chain, classifying them according to the height of the dissolution teeth and, hence, to the resulting morphology. The sedimentary burial stylolites are described as generally smooth wave-type structures but are characterized by slightly rough sharp-peak morphologies in grain-supported carbonate rocks. Tectonic burial stylolites are described as rough seismogram-type surfaces with dissolution teeth larger than sedimentary burial ones. For the purpose of investigating the compaction processes active during the burial diagenesis, in this work, we then consider only the sedimentary burial bed-parallel stylolites, aiming at providing new insights on the time-dependent evolution of the structural architecture of the studied fractured carbonates.

2. Geological Setting

The southern Apennines fold-and-thrust belt (FTB) started to form during late Oligocene–early Miocene due to the collision between Africa and the Eurasian plates and the intervening Adria-Apulia plate [32]. This deformation determined the progressive involvement of Mesozoic sedimentary units in a compressional tectonic regime, and formation of an east-verging FTB by means of mixed thin-skinned and thick-skinned tectonics [33]. The latter units include the terrigenous and mixed siliciclastic/carbonate infills of the Sicilide–Liguride Basin and of the Lagonegro Basin, the Apennine platform carbonates, the Apulian platform carbonate, and the terrigenous syn-orogenic flysch deposited in the foreland and thrust-top basins [28,32,34]. Tectonic stacking

of the aforementioned units caused the sandwiching of the Apennine Platform in between the overlying Sicilide–Liguride and the underlying Lagonegro units. Altogether, this tectonic wedge overrode the Apulian Platform [35]. Particularly, the basinal Liguride and Sicilide units overthrust during early Miocene the Apennine Platform; subsequently, the two aforementioned units overthrust during Tortonian the already duplexed basinal Lagonegro units [28,32]. The foredeep and thrust-top basins that formed along the evolving FTB during this timelapse marked the various tectonic stages that characterized the east-directed migration of contractional deformation [36].

Due to the aperture of the Tyrrhenian back-arc basin, and the concomitant gravitational collapse of the collisional belt, starting from late Pliocene, the tectonic wedge was subjected to extension [37–40]. At first, the belt was dissected by low-angle normal faults likely due to gravity-driven reactivation of pre-existing thrust faults; then, during Quaternary, the belt was dissected by high angle transtensional faults that caused exhumation of the allochthonous units from depth [32,41–44].

The present study focuses on the carbonates from the Apennine Platform, which developed during Mesozoic along the western region of the Tethys Ocean [28,45]. At a regional scale, the following three main stratigraphic units were documented within this carbonate succession: (1) the Capri-Bulgheria unit, which includes Triassic to Jurassic shallow-water transitional carbonate facies, Cretaceous to Miocene marls, and resedimented carbonates deposited along the western margin of the carbonate platform; (2) the Alburno-Cervati unit, which includes Upper Triassic to Cretaceous shallow-water limestones, Miocene slope carbonates, and terrigenous deposits, and represents the internal portion of the ancient carbonate platform; (3) the Monti della Maddalena unit, which is constituted by transitional carbonate facies deposited along the eastern margin of the ancient carbonate platform.

Viggiano Mt.

Viggiano Mt. is located in the High Agri Valley of the Basilicata Region, Italy (Figure 1), which is a tectonic intra-montane basin infilled with Quaternary fluvio-lacustrine sediments. The High Agri Valley basin is bound by high-angle, WNW-ESE, and NW-SE striking transtensional faults forming the East Agri Fault System (EAFS) and the Monti della Maddalena Fault Systems (MMFS) (Figure 1b). Viggiano Mt. is dissected by high-angle faults pertaining to the EAFS, and comprises Apennine platform carbonates that overrode the Lagonegro II unit by means of an east-verging low-angle thrust fault (Figure 1b). The Viggiano Mt. succession, belonging to the Alburno-Cervati unit, consists of Lower Jurassic wackestones, packstones, and grainstones originally deposited in a low-energy lagoonal environment. The latter carbonates contain bivalve shells (*Lithiotis*), foraminifera (*Siphovalvulina* sp., *Pseudocyclammina liassica*), and green algae (*Palaeodasycladus mediterraneus*). The low-energy carbonates are topped by oolitic grainstones, which were originally deposited on a carbonate ramp rimmed by sand shoals [30,46].

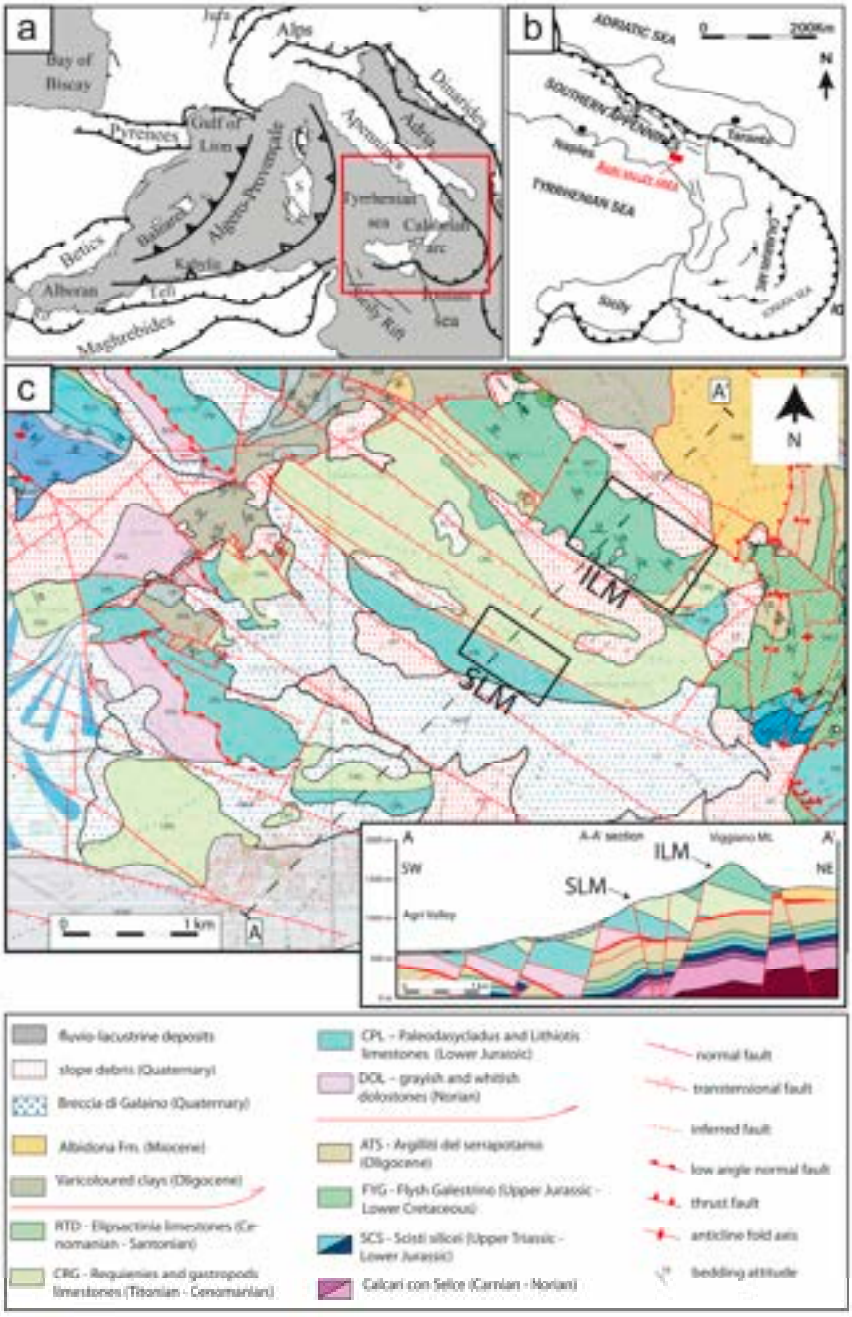

Figure 1. Geological map of the study area. (**a**) Regional overview of the study area. (**b**) Schematic map of the southern Apennine FTB, with the Agri Valley location and study area location. (**c**) Geological map of the Viggiano Mt. area [39], with the locations of the SLM (Scarlo Mt. Mia) and ILM (Il Monte) study sites and the SW-NE geological cross-section of the Viggiano Mt. area.

3. Methods

The petrographic characterization of the Viggiano limestone was carried out in order to obtain information on the carbonate microfacies and the bed-parallel pressure solution surfaces. The methodologies used are set out as follows:

3.1. Field Analyses

The laboratory work was subsequent to the field stratigraphic analysis of the carbonates exposed at the two sites and detailed mesoscale structural analysis of the aforementioned pressure solution surfaces.

The Upper Jurassic carbonates consist of alternations of depositional breccias and lagoonal mudstones/wackestones. Through not-brecciated portions of green algae (*Thaumatoporella parvovesciculifera*, *Cayeuxia piae*), calcified cyanobacteria (*Lithocondium aggregatum*), gastropods, bivalves, and various foraminifera species (*Miliolidae* sp., *Conicospirillina basiliensis*, *Pseudocyclammina lituus)* have been documented [46]. The youngest portion of Viggiano Mt. consists of Cretaceous limestones made up of carbonate grainstones, rudstones, floatstone with rudist fragments, and sporadic mudstones. These rocks were originally deposited during Albian–Cenomanian in a high-energy shelf environment close to the platform margin [30,46]. At Viggiano Mt., the present work focuses on the carbonated

exposed at two sites labeled as Scarrone la Macchia (SLM) and Il Monte (ILM), respectively (Figure 1).

3. Methods

The petrographic characterization of the Viggiano limestone was carried out in order to obtain information on the carbonate microfacies and the bed-parallel pressure solution surfaces. The methodologies used are set out as follows:

3.1. Field Analyses

The laboratory work was subsequent to the field stratigraphic analysis of the carbonates exposed at the two sites and detailed mesoscale structural analysis of the aforementioned pressure solution surfaces.

3.2. Petrographic and Microfacies Observations

The petrographic analysis was conducted by using an optical microscope (Leitz Laborlux 12 Pol, Esselte Leitz GmbH & Co KG, Stuttgart, Germany) associated with Zen 2012 SP1 software for the acquisition of photomicrographs at the Department of Earth and Marine Sciences of University of Palermo. The textural classifications of microfacies followed Dunham [47] and Embry and Klovan (1971). The classification of pressure solution surfaces followed Flugel [3] and Koehn et al. [22].

3.3. Cathodoluminescence Observations

A cold-stage CL instrument (CCL 8200 Mk3, Cambridge Image Technology Ltd., Hatfield, UK) present at the Department of Geosciences of University of Padua, Italy, was used to obtain data on the several generations of cements and the crosscutting relationship with the pressure solution features [48]. The CL beam was operated at 20 kV beam energy and 200–300 mA beam current. Images were obtained with a Nikon petrographic microscope (Nikon Corporation, Tokyo, Japan).

4. Results

The analysis of the diagenetic features in samples collected from the two sites is meant to assess the relations among textures, cementation, and pressure solution processes. In particular, the results of petrographic observations associated with CL analysis permitted the distinction of multiple generations of calcite cement. For the Scarrone la Macchia site, results of field stratigraphic and structural analyses are also reported for the well-layered and oolitic units, which are investigated in great detail.

4.1. Scarrone la Macchia (SLM) Site

The exposed carbonates at the SLM site are sub-divided into two informal units [30] (Figure 2a,c). Starting from the base, the well-layered unit consists of about 13 m thick shallow-water limestone. There, three main facies are differentiated (Figure 2) as (a) algal grainstone/packstone characterized by abundant calcareous algae (*Palaeodasycladus mediterraneus* and *Thaumatoporella parvovesiculifera*) associated with benthic foraminifera (Figure 3a,b) (this facies is typical of a moderate-energy shallow marine lagoonal environment); (b) benthic foraminifera wackestone, characterized by an association of benthic foraminifera (including *Haurania* sp., *Siphovalvulina* sp., *Lituosepta* sp.) interpreted as a moderate- to low-energy lagoonal environment (Figure 3c,d); (c) marly layers.

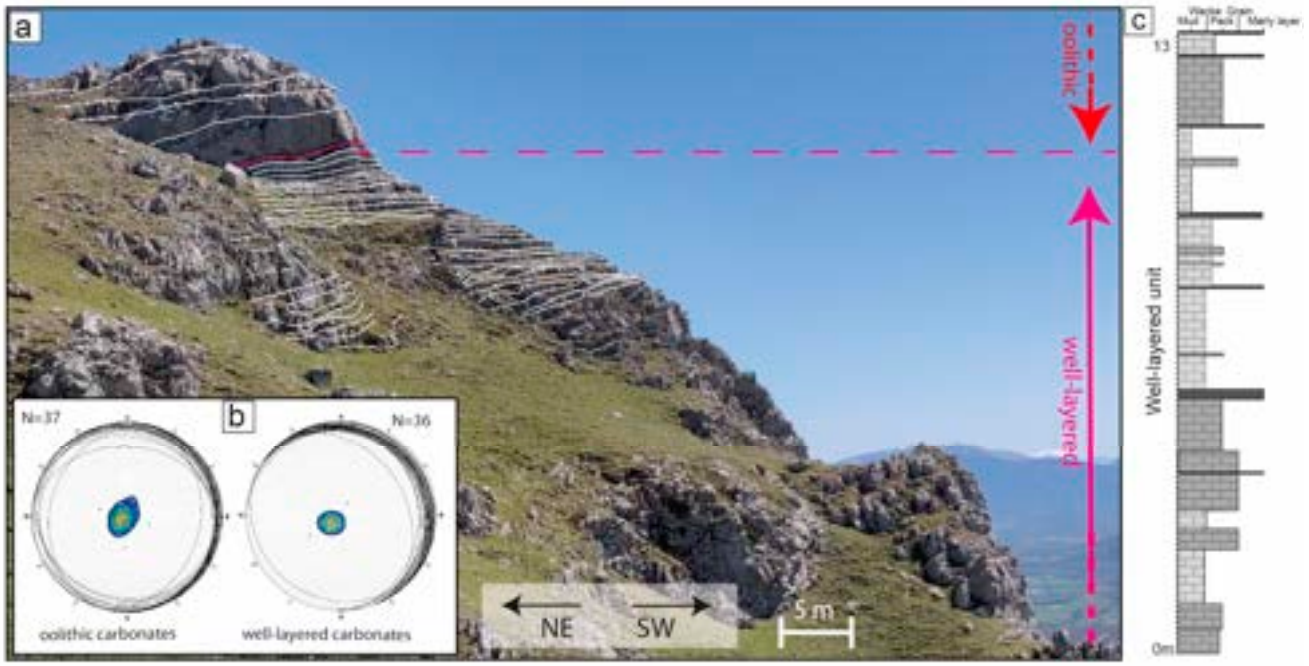

Figure 2. (**a**) Outcrop views of the SLM in which the well-layered and oolitic units are differentiated. (**b**) Bedding attitude of SLM. (**c**) Detailed stratigraphic log showing the facies texture of the well-layered unit of the SLM site.

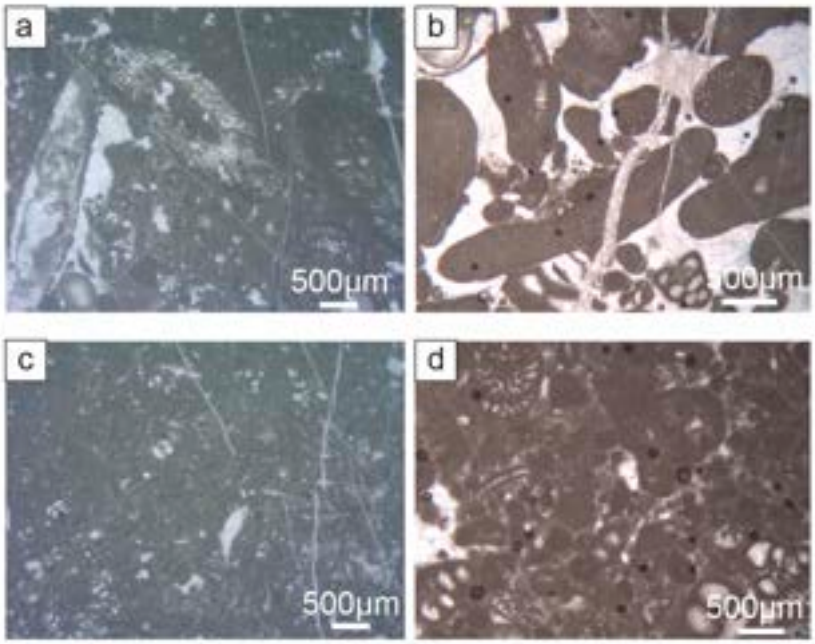

Figure 3. Microfacies of the well-layered unit of Scarrone la Macchia: (**a**) Packstone with *Paleodasycladus mediterraneus* and benthic foraminifera. (**b**) Grainstone with algae and benthic foraminifera. (**c**) Wackestone with benthic foraminifera. (**d**) Wackestone/packstone with *Siphovalvulina* sp., *Haurania deserta*.

4.1.1. Diagenetic Features

Capping the well-layered unit, the 17 m thick grain-supported unit consists of oolitic limestones (Figure 2a,c). The results of microfacies analyses show that it includes carbonate grainstone and packstone with ooids (0.5 to 1 mm in size), oncoids (>1 mm), and algal lumps. In some cases, the ooids show an obliteration of the laminae due to intense micritization. Their nuclei are made of skeletal grains, peloids, and, in rare cases, siliciclastic sand grains.

On the whole, SLM carbonate—a first generation rim of isopachous cement—is documented around major cavities. These rims are hundreds of microns thick and made of elongated crystals of radiaxial fibrous type. These cements are dark under cathode light,

4.1.1. Diagenetic Features

On the whole, SLM carbonate—a first generation rim of isopachous cement—is documented around major cavities. These rims are hundreds of microns thick and made of elongated crystals of radiaxial fibrous type. These cements are dark under cathode light, and occur only in the carbonate packstones and wackestones of the well-layered unit (Figure 4a,b). Coevally, in the carbonate grainstones of both well-layered and oolitic units, cements consist of ca. 50-micron-thick isopachous calcite rims, which localize between adjacent grains as meniscus cements (Figure 4c,e,f). These cements are dark under cathode light (Figure 4d). The second generation of cements is characterized by blocky calcite, which is often densely twinned and appears either dark or very dull under cathode light (Figure 4a–d). Thin calcite may also exhibit rhythmic luminescence. The carbonate cements infilled all primary porosity and WNW-ESE high-angle veins.

On the whole, SLM carbonate—a first generation rim of isopachous cement—is documented around major cavities. These rims are hundreds of microns thick and made of elongated crystals of radiaxial fibrous type. These cements are dark under cathode light, and occur only in the carbonate packstones and wackestones of the well-layered unit (Figure 4a,b). Coevally, in the carbonate grainstones of both well-layered and oolitic units, cements consist of ca. 50-micron-thick isopachous calcite rims, which localize between adjacent grains as meniscus cements (Figure 4c,e,f). These cements are dark under cathode light (Figure 4d). The second generation of cements is characterized by blocky calcite, which is often densely twinned and appears either dark or very dull under cathode light (Figure 4a–d). Thin calcite may also exhibit rhythmic luminescence. The carbonate cements infilled all primary porosity and WNW-ESE high-angle veins.

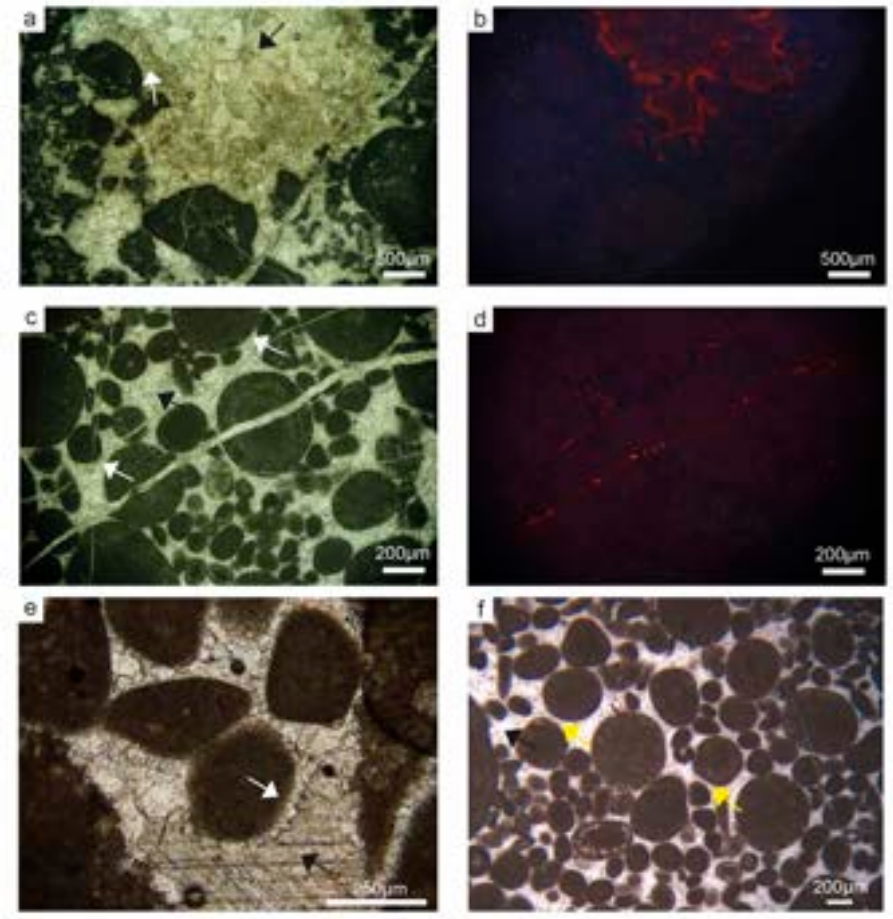

Figure 4. (**a**) Plain polarized light image of the well-layered unit showing radiaxial fibrous cements (white arrow) and blocky cements (black arrow). (**b**) Same image of (**a**) under CL. (**c**) Plain polarized light image of the oolitic unit showing isopachous cements (white arrow) and blocky cements (black arrow). (**d**) Same image of (**c**) under CL. (**e**) Plain polarized light image of a grain-supported facies in the well-layered unit showing isopachous cements (white arrow) and blocky cements (black arrow). (**f**) Plain polarized light image of the oolitic unit showing meniscus cements (yellow arrow) and blocky cements (black arrow).

4.1.2. Pressure Solution Features

According to the single lithofacies, pressure solution features show peculiar morphologies and specific crosscutting relations with the calcite cements. The grain-supported facies of both well-layered and oolitic units are characterized by dissolution features localized at the grain contacts; concavity-convexity, sutured contacts (Figure 5). These features have a limited lateral extension of a few millimeters, which is the function of grain size and, hence, of the grain contact area, while the dissolution teeth are not well-developed (Figure 5). The bed-parallel stylolites show rough morphologies, and are classified as sharp-peak [1,22] (Figure 6a,b). These stylolites dissolve both carbonate grains and calcite cements (Figure 6a,b). Sometimes, the stylolites are filled with

Geosciences **2024**, *14*, x FOR PEER REVIEW 8 of 18
Geosciences **2024**, *14*, x FOR PEER REVIEW 8 of 18

of grain size and, hence, of the grain contact area, while the dissolution teeth are not well-developed (Figure 5). The bed-parallel stylolites show rough morphologies, and are classified as sharp-peak [1,22] (Figure 6a,b). These stylolites dissolve both carbonate grains and calcite cements (Figure 6a,b). Sometimes, the stylolites are filled with residual material, which consists of clay and/or oxides, and are non-luminescent under CL (Figure 6b). Occasionally, these features may include a partially preserved porosity (Figure 6b). In the mud-supported carbonates of the well-layered unit, the pressure solution surfaces consist of stylolites with irregular to rough morphologies, which are classified as rectangular to wave-like types [1,22]. These features either dissolve or confine against the high-angle WNW-ESE veins, and contain films of brownish-reddish residual material (Figure 6e,f).

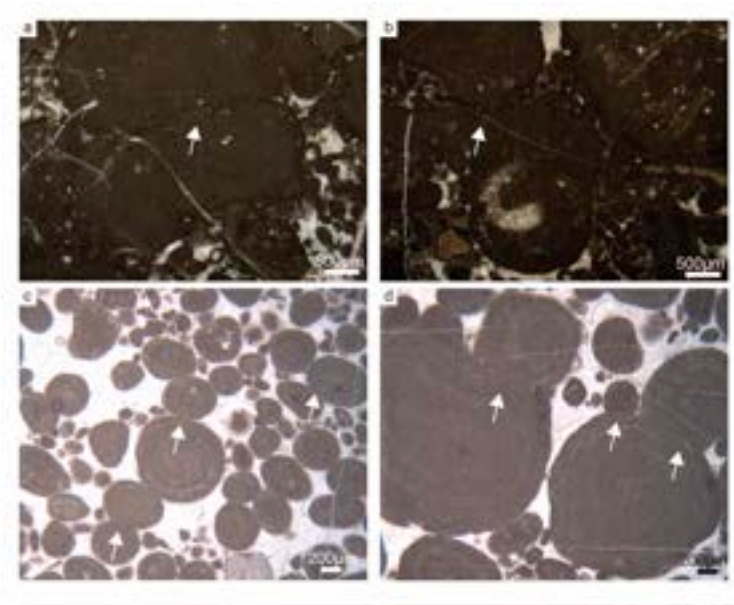

Figure 5. Plain polarized light image showing grain contact seams (white arrows) of the grain supported facies in the well-layered unit (**a**,**b**) and in the oolitic unit (**c**,**d**).

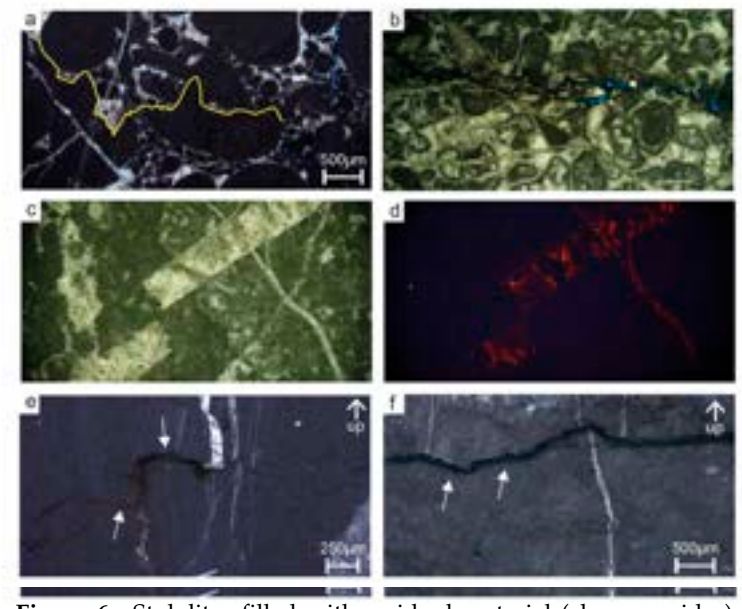

Figure 6. Stylolites filled with residual material (clay or oxides) that under CL are dark (**a**,**b**). Sometimes they have a partially preserved porosity (**c**,**d**). (**e**) Bed-perpendicular WNW-ESE veins dissolved by a rectangular-type stylolite (see white arrows) within mudstone in the well-layered unit. (**f**) Bed-perpendicular WNW-ESE veins abutting against a wave-type stylolite (see white arrows) within mudstone in the well-layered unit.

Geosciences 2024, 14, x FOR PEER REVIEW 9 of 18

(f) Bed perpendicular WNW-ESE veins abutting against a wave type stylolite (see white arrows) within mudstone in the well-layered unit.

4.2. Il Monte (ILM) Site

The succession exposed at the ILM site consists of 67 m of massive carbonate (Figure 7a–c). The facies textures are rudstones and floatstones, which include fragments of rudist bivalves (*Radiolitidae* and *Caprinae*), common larger foraminifera (orbitolinids), corals, and intraclasts made up of clotted peloidal micrite (Figure 8). Microbial encrustations are commonly documented around skeletal and non-skeletal grains and several grains are intensely micritized. The benthic foraminifera and rudist associations are consistent with an Upper Cretaceous age according to the biozonal schemes proposed by [49,50]. Recent studies argued for an Albian–Cenomanian age due to the association between Radiolitidae, *Concorbitolina conica*, *Sulpingoporella turgida*, and Caprinidae [46].

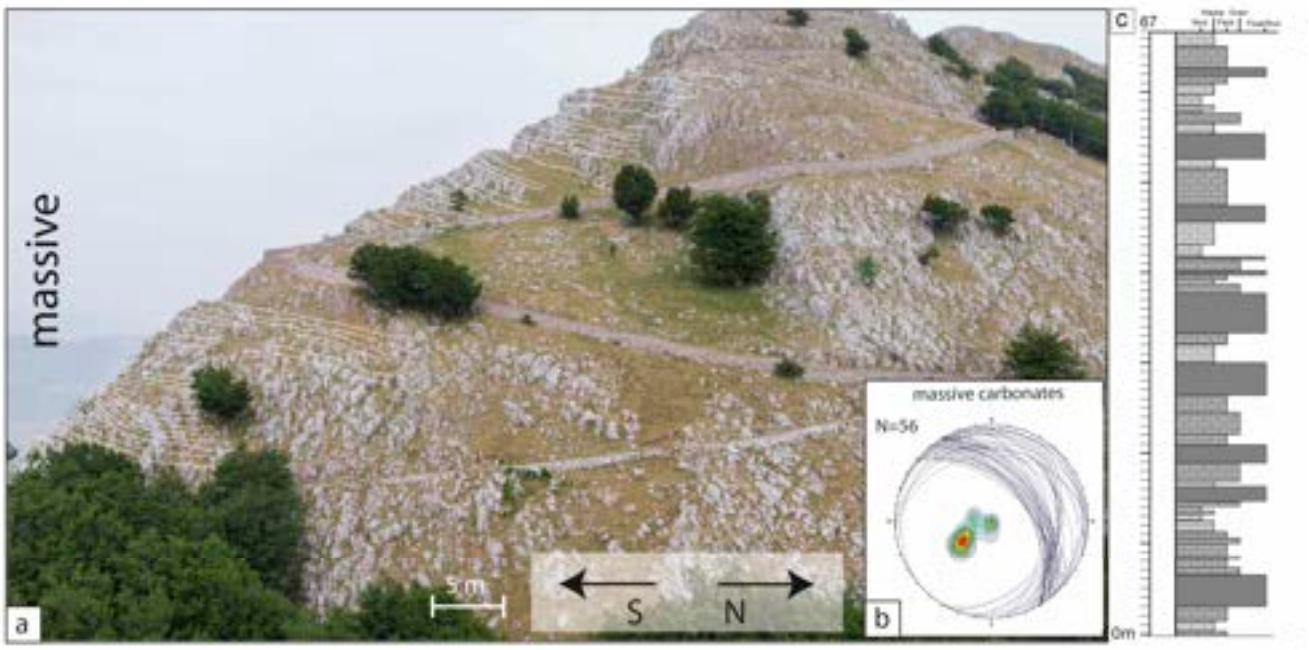

Figure 7. (**a**) Outcrop view of ILM study site; (**b**) bedding attitude measured along the section; (**c**) stratigraphic logs of ILM with the location of analyzed samples.

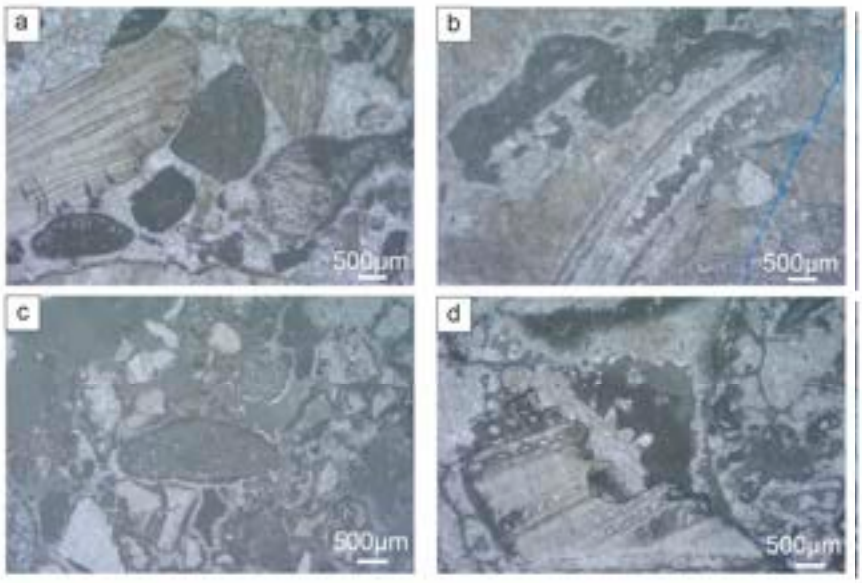

Figure 8. (**a**–**d**) Microfacies of the Il Monte section characterized by floatstone/rudstone with fragments of rudist shells and orbitolinids.

Figure 8. (**a**–**d**) Microfacies of the Il Monte section characterized by floatstone/rudstone with fragments of rudist shells and orbitolinids.

4.2.1. Diagenetic Features

The diagenetic features consist of a first generation of radiaxial fibrous cements, which are dark under CL but also cut by luminescent spots (Figure 9a,b). These spots are likely defects of the crystals. In some cases, the first generation of cements consists of dog-tooth cements, which are dull under CL (Figure 9c,d). The fine-grained carbonate sediments within the primary cavities, often forming geopetal partial infills, post-date the precipitation of these dog-tooth like cements (Figure 9c,d). The second generation of cements consists of blocky calcite, which infills veins and all primary pores. Under CL, these cements show zonation due to alternations of layers with a dull to bright luminescence (Figure 9e,f). The skeletal grains, which mainly consist of rudist fragments, are fully dark under CL, apart for those skeletal grains in which the shell skeleton was substituted by a mosaic of blocky calcite crystals (Figure 9e,f). Differently, the micritic rims and microbial carbonates are dull luminescent under CL (Figure 9e,f).

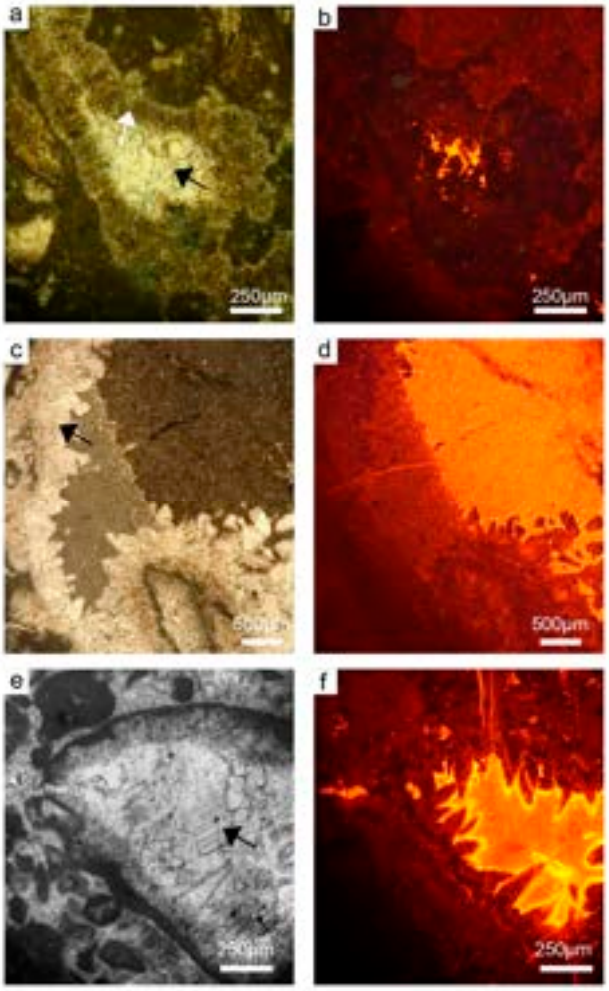

Figure 9. (**a**) Plain polarized light image showing the radiaxial fibrous cements (white arrow) and blocky cements (black arrow). (**b**) Same image of (**a**) under CL. (**c**) Plain polarized light image showing dog-tooth cements (black arrow) and sediment infill. (**d**) Same image of (**c**) under CL. (**e**) Polarized images showing blocky cements (black arrow). (**f**) Same image of (**e**) under CL.

4.2.2. Pressure Solution Features

At the microscale, no grain contact seams are observed and the pressure solution features only include stylolites. The morphology of these stylolites is commonly rough. In the rudstone carbonate facies, they show tiny pinning teeth as high as a few tens of µm (Figure 10a,b). According to Koehn et al. [22], the stylolites are classified as a sharp-peak type. Differently, stylolites with teeth as high as 100–200 µm are documented within the

4.2.2. Pressure Solution Features

At the microscale, no grain contact seams are observed and the pressure solution features only include stylolites. The morphology of these stylolites is commonly rough. In the rudstone carbonate facies, they show tiny pinning teeth as high as a few tens of μm (Figure 10a,b). According to Koehn et al. [22], the stylolites are classified as a sharp-peak type. Differently, stylolites with teeth as high as 100–200 μm are documented within the floatstone carbonate facies (Figure 10c,d). Wave-like stylolites occur only in the carbonate facies, including micrite (Figure 10e). The stylolites dissolve skeletal fragments, carbonate grains (Figure 10a), calcite cements (Figure 10b,c), and WSW-ENE striking high-angle veins (Figure 10d). The stylolites contain a residual reddish-brownish material, and/or are partially open (Figure 10e,g). Occasionally, under CL the residual sediment appears bright luminescent (Figure 10f).

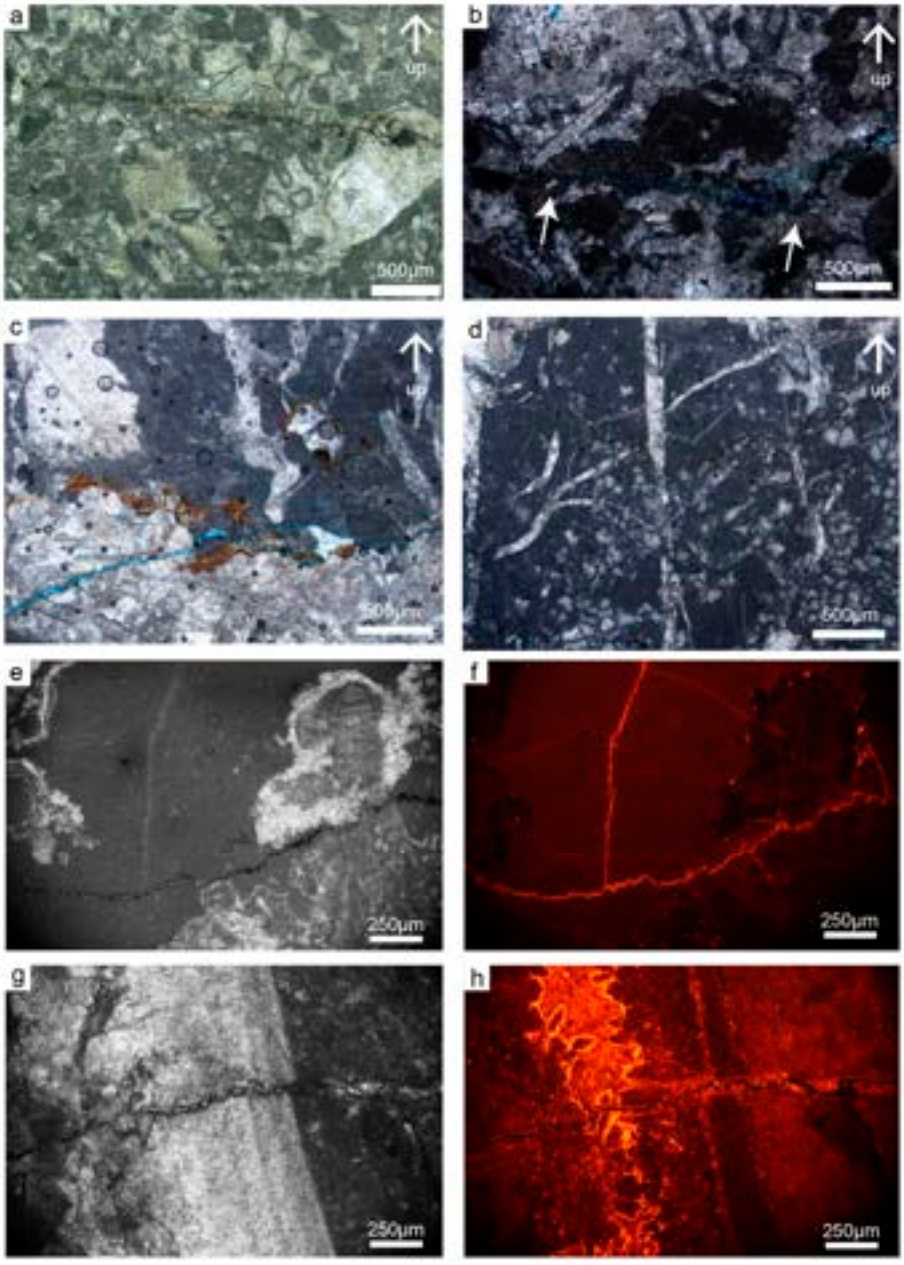

Figure 10. (**a**,**b**) sharp-peak stylolites characterized by tiny, pinning teeth as high as few tens of μm dissolving calcite cements (white arrows in (**b**)). (**c**,**d**) sharp-peak stylolites characterized by high roughness that dissolves both carbonate grains and cements. These stylolites contain residual material. (**e**,**f**) wave-like stylolites in the carbonate facies containing micrite. Under CL, the residual sediment appears bright luminescent. (**g**,**h**) Stylolite dissolving both carbonate bioclasts and cements. The stylolites is partially open.

5. Discussion

It is known that chemical compaction is facies-dependent, so that the nucleation pressure solution surface has a tight relation with the texture of carbonate rocks [3]. Starting

from this consideration, on the basis of the microfacies characterization of the studied carbonates, we first assess the settings in which the carbonate sediments were originally deposited, and then the main diagenetic processes and associated burial conditions that occurred during the Meso–Cenozoic in the Apennine Platform.

5.1. Depositional Setting

The carbonate described at the SLM site was originally deposited in an inner-platform depositional environment, which was characterized by presence of a carbonate sandy margin protecting the lagoon [30]. Furthermore, the association of benthic foraminifera (including *Haurania* sp., *Siphovalvulina* sp., *Lituosepta* sp.) and calcareous algae (*Palaeodasycladus mediterraneus* and *Thaumatoporella parvovesiculifera*) is consistent with an upper Sinemurian–Pliensbachian age, according to the biozonal scheme proposed by [50,51].

Focusing on the facies distributions exposed along the well-layered unit, they are indicative of a moderate-to-low energy lagoonal environment. The vertical repetition of algal packstone/grainstone, benthic foraminifera wackestone, and marly layers suggests a cyclic deposition controlled by sea level fluctuations [3]. A Similar depositional environment characterizes the Lower Jurassic carbonate platform sedimentation of Western Tethys and it has been described both in the southern Alps [52] and in the Apennines [53].

The upward transition from well-layered to oolitic units was previously interpreted as being due to a transgression phase and the consequent landward migration of the paleo sand margin [30]. This lithofacies sequence is now interpreted as likely being due to sea level rise, which occurred close to the Pliensbachian–Toarcian transition [53,54]. We note that this transition was accompanied by a large-scale mass extinction event, also documented by the biostratigraphic data collected from the SLM site [30].

Considering carbonates exposed at the ILM site, according to microfacies analyses, they were interpreted as being originally deposited in a lagoonal environment punctuated by rudist patch reefs [30]. The original data reported in this work suggest that the formation of rudstone and floatstone is related to wave actions, which erode and rework the patch reefs. Furthermore, the abundance of mud in the rocks is interpreted as being due to the different hydrodynamic energy levels during deposition [3]. Similar depositional environments characterized by lagoonal/tidal flats close to the platform margin have also been described in northern Sicily by [55].

5.2. Diagenetic Evolution

The following analysis of the diagenetic features is based on the aforementioned description and classification of the different generations of cements. The cement generations, and hence the resulting carbonate textures, are then compared with the different types of stylolites and pressure solution seams in order to assess any possible influence exerted by carbonate textures on pressure solution processes associated with burial diagenesis.

At the SLM site, the mud-supported facies of the well-layered carbonates include radiaxial fibrous cements that are not luminescent under CL, suggesting that their precipitation occurred under oxidizing conditions in the marine phreatic diagenetic environment [3,48]. Being dark under CL, the isopachous cement rims documented in the grain-supported carbonates of either well-layered or oolitic units also formed in a marine phreatic environment [3,48]. Differently, the meniscus cements precipitated in a vadose environment above the paleo-water table [3]. This condition likely occurred during subaerial exposures of the platform's sandy margin, which was related to high-frequency sea level fluctuations [3]. Finally, the blocky cements precipitated as a late infill within the remaining pore space. Their zonation, from dark to dull luminescence, indicates a shallow burial diagenetic environment [3,48].

The diagenetic features documented for the carbonates exposed at the SLM site may therefore be ascribed to diagenetic environments associated with marine phreatic to shallow burial. In detail, in the marine phreatic diagenetic environment, the precipitation of the first generation of calcite cements (both radiaxial fibrous and isopachous) occurred, while,

during the sedimentary burial, the precipitation of blocky calcite occurred, filling the remaining pore space. At this stage, the early cementation of carbonates predated the beginning of the pressure solution processes. In fact, in the grain-supported carbonates pertaining to either well-layered or oolitic units, the bed-parallel stylolites dissolved both carbonate grains and calcite cements. The burial history extrapolated by diagenetic analyses is in accordance with the recent data reported by Manniello et al. [19], who calculated a sedimentary burial of ca. 1.4–1.6 km in the southern Apennines before the onset of Miocene–Pliocene thrusting tectonics.

As a whole, we observe a relationship between the stylolite type and the facies texture of the host rock inherited from the depositional environment. In particular, in the mud-supported facies, stylolites occur as wave-like to rectangular types, while in the grain-supported facies, they appear as sharp-peak types (Figure 11). Independently from the bed thickness, the longest stylolites are documented within the mud-supported carbonate beds, where they can reach lengths up to ca. 100 cm [19]. Contrarily, in the grain-supported facies, the bed-parallel stylolites are characterized by a very limited lateral extension with values ranging between 3 cm and 15 cm, as calculated by Manniello et al. [19]. As observed by Rutichelli et al. [10], the bed-parallel stylolites that have greater lateral extension have a key role in the circulation of the fluids, particularly poorly faulted shallow-water limestones.

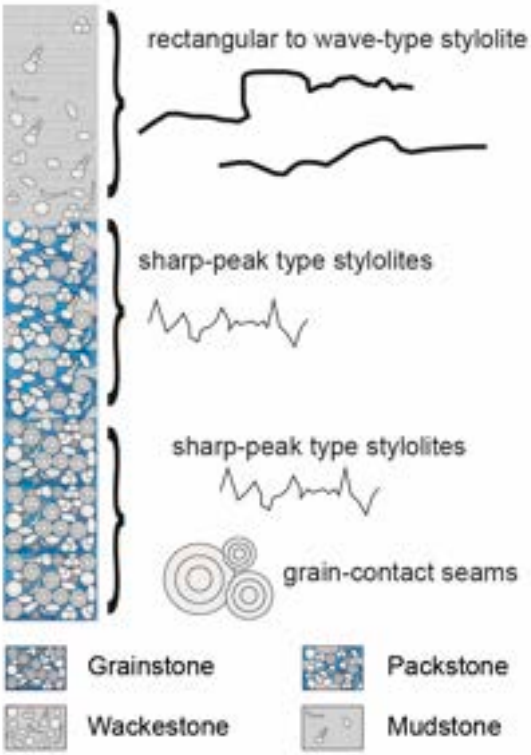

Figure 11. Deepening upward cycle characterizing the facies stacking of the well-layered unit in the SLM site. On the right side is the classification of stylolites in relationship to the facies textures.

Our interpretation is in agreement with those proposed for other limestone successions, where the authors documented that finer grain sizes favored the pressure solution processes [1,10,16,56].

It has been postulated that the clay minerals present in the finer grained limestones catalyzed pressure solutions through the diffusion of dissolved host rock along thin water films [57–59], and/or due to differences in the electrochemical potential with the dissolving minerals [60,61]. We note that the mud-supported carbonates exposed at the SLM site are characterized by a greater amount of clay with respect to the grain-supported ones, which supports the former postulation.

Regarding the estimation of compaction, Beaudoin et al. [16] first claimed that analysis of the nucleation processes of bed-parallel stylolites can be useful in estimating the burial depth of the carbonates. Later on, Zhou et al. [1] proposed quantification of the burial depth on the basis of the maximum amplitude of the stylolite teeth dissolving grain-supported carbonates. According to Koehn et al. [62] and Ebner et al. [63], the rougher stylolites (e.g., sharp-peak) allow a good compaction estimation, while the smoother stylolites (e.g., wave-type stylolites) can offer compaction underestimation because the height of the dissolution teeth is not representative of the amount of dissolution due to their non-linear growth.

Regarding the estimation of compaction, Beaudoin et al. [16] first claimed that analysis of the nucleation processes of bed-parallel stylolites can be useful in estimating the burial depth of the carbonates. Later on, Zhou et al. [1] proposed quantification of the burial depth on the basis of the maximum amplitude of the stylolite teeth dissolving grain-supported carbonates. According to Koehn et al. [62] and Ebner et al. [63], the rougher stylolites (e.g., sharp-peak) allow a good compaction estimation, while the smoother stylolites (e.g., wave-type stylolites) can offer compaction underestimation because the height of the dissolution teeth is not representative of the amount of dissolution due to their non-linear growth.

Considering that the length of single teeth represents the minimum compaction [64], we now take into account data recently measured by Manniello et al. [19] for the studied SLM carbonates. In detail, we consider the data related to the bed-parallel stylolites formed during the sedimentary burial, excluding those related to the tectonic burial. The sharp-peak stylolites show a height of dissolution teeth between 0.5 and 0.1 mm and a width between 0.2 and 0.05 mm. The wave/rectangular stylolites show a height of dissolution teeth between 0.18 and 0.01 mm and a width between 0.1 and 0.01 mm.

To estimate the amount of compaction, we consider the linear intensity P10 (P10, number of stylolites per unit length of 30 cm) calculated by Manniello et al. [19] for the same carbonates but exclude the data relating to the tectonic thrusting phase.

The P10 values correspond to an average of 2,4 stylolites/30 cm. When multiplying it with the highest values of the dissolution teeth (0.5 mm), we obtain a minimum compaction value of 1.2 mm per 30 cm, corresponding roughly to a 4% volume loss. These data are slightly lower than commonly reported in the literature, which range from ca.15% [65] to ca. 40% [22,66], probably due to the early cementation described for SLM carbonates. Data from the literature assert that shallow-water carbonates can be resistant to compaction up to a depth of 700 m [3].

Focusing on the Cretaceous carbonates exposed at the ILM site, according to the results of petrographic and CL analyses, we document that the two first generations of cements consist of radiaxial fibrous and dog-tooth calcite precipitated in marine diagenetic environments [3]. Accordingly, we envision that the dissolution of aragonite rudist shells started during the early burial stages, concurrent with the preservation of moldic porosity that was partially still open. We propose that the primary intergranular pores were than partially filled by blocky cements during shallow burial conditions before the inception of pressure solution processes. Formation of the bed-parallel stylolites started once pores were almost completely filled by the blocky cements, as shown by the crosscutting relations documented in this work (cf. Figure 10). Later on, during deeper burial conditions [19], the occurrence of large grains within the poorly sorted carbonates favored the formation of sharp-peak-type stylolites, which are characterized by low lateral distribution and high amplitudes. A similar geometry was observed in the large grains of Cretaceous coralline limestones of Spain [23]. There, the bed-parallel stylolites are characterized by moderate amplitudes and wavelengths and smaller spacing values with respect to those within rocks with smaller grain sizes.

6. Conclusions

Considering the potential influence that stylolites have on the circulation of fluids, this study allows us to predict the potential reservoir properties of shallow-water limestone, starting with the analysis of the depositional environment and, therefore, of the facies texture and diagenetic processes.

The data collected at the two sites, SLM and ILM, respectively, allow to point out how the depositional environment and diagenetic processes play a key role in the nucleation of pressure solution process. The CL data account for diagenesis that occur in a shallow burial stage after marine/meteoric cementation. The early cementation, typical of a shallow-water carbonate environment, forbids compaction during burial and the formation of pressure solution features.

We observe how the original texture of the rock controls the formation of pressure solution features during the sedimentary burial, which can be summarized as follows:

- The high energy facies characterized by low mud content and represented by grainstone/packstones are less compacted due to early cementation. In this case, the pressure solution processes result in grain contact seams and stylolites. In detail, the bed-parallel stylolites are characterized by rougher morphology and show a low lateral extension. Moreover, in the case of larger grains (>2 mm, e.g., rudstone), the nucleation and diffusion of bed-parallel stylolites is inhibited, and pressure solution features are represented only by grain contact seams.
- The low energy facies, characterized by a greater presence of mud and represented by wackestone/mudstone, lack grain contact seams, while bed-parallel stylolites are characterized by smooth morphology and good lateral extension. This is favored by the presence of carbonate mud that catalyzes the pressure solution processes, as evidenced by the greater amount of residual material. This type of bed-parallel stylolites promotes the circulation of fluids, thanks also to their lateral extension.

Author Contributions: Field survey and data acquisition, C.M., A.P., F.A. and S.T.; Lab analyses, S.T., C.M. and N.P.; Data interpretations, C.M., A.P., F.A., S.T. and N.P.; Writing—original draft, S.T., F.A. and C.M.; Writing—editing, S.T., F.A. and C.M. Writing—review, S.T., F.A., C.M. and N.P.; Illustrations, S.T. and C.M. All authors have read and agreed to the published version of the manuscript.

Funding: This work was carried out with the financial support of the Reservoir Characterization Project (www.rechproject.com) by F.A., University of Palermo (R4D14-P5F5RISS_MARGINE) by S.T. and University of Padova, by N.P.

Data Availability Statement: All data have been reported in the text.

Conflicts of Interest: The authors declare that they have no known competing financial interests or personal relationships that could have appeared to influence the work reported in this paper.

References

1. Zhou, L.; Wang, G.; Hao, F.; Xu, R.; Jin, Z.; Quan, L.; Zou, H. The Quantitative Characterization of Stylolites in the Limestone Reservoirs of the Lower Triassic Feixianguan Formation, Northeastern Sichuan Basin: Insights to the Influence of Pressure Solution on the Quality of Carbonate Reservoirs. *Mar. Pet. Geol.* **2022**, *139*, 105612. [CrossRef]
2. Wong, P.K.; Oldershaw, A. Burial Cementation in the Devonian, Kaybob Reef Complex, Alberta, Canada. *J. Sediment. Petrol.* **1981**, *51*, 507–520. [CrossRef]
3. Flugel, E. *Microfacies of Carbonate Rocks Analysis, Interpretation and Application*; Springer: Berlin/Heidelberg, Germany; New York, NY, USA, 2004.
4. Rahim, H.u.; Ahmad, W.; Jamil, M.; Khalil, R. Sedimentary Facies, Diagenetic Analysis, and Sequence Stratigraphic Control on Reservoir Evaluation of Eocene Sakesar Limestone, Upper Indus Basin, NW Himalayas. *Carbonates Evaporites* **2024**, *39*, 15. [CrossRef]
5. Khitab, U.; Umar, M.; Jamil, M. Microfacies, Diagenesis and Hydrocarbon Potential of Eocene Carbonate Strata in Pakistan. *Carbonates Evaporites* **2020**, *35*, 70. [CrossRef]
6. Choquette, P.W.; James, N.P. Diagenesis# 12. Diagenesis in Limestones-3. The Deep Burial Environment. *Geosci. Can.* **1987**, *14*, 3–35.
7. Marshak, S.; Engelder, T. Development of Cleavage in Limestones of a Fold-Thrust Belt in Eastern New York. *J. Struct. Geol.* **1985**, *7*, 345–359. [CrossRef]
8. Korneva, I.; Tondi, E.; Agosta, F.; Rustichelli, A.; Spina, V.; Bitonte, R.; Di Cuia, R. Structural Properties of Fractured and Faulted Cretaceous Platform Carbonates, Murge Plateau (Southern Italy). *Mar. Pet. Geol.* **2014**, *57*, 312–326. [CrossRef]
9. Rustichelli, A.; Tondi, E.; Agosta, F.; Cilona, A.; Giorgioni, M. Development and Distribution of Bed-Parallel Compaction Bands and Pressure Solution Seams in Carbonates (Bolognano Formation, Majella Mountain, Italy). *J. Struct. Geol.* **2012**, *37*, 181–199. [CrossRef]
10. Rustichelli, A.; Tondi, E.; Korneva, I.; Baud, P.; Vinciguerra, S.; Agosta, F.; Reuschlé, T.; Reuschlé, T. Bedding-Parallel Stylolites in Shallow-Water Limestone Successions of the Apulian Carbonate Platform (Central-Southern Italy). *Ital. J. Geosci.* **2015**, *134*, 513–534. [CrossRef]
11. Laronne Ben-Itzhak, L.; Aharonov, E.; Karcz, Z.; Kaduri, M.; Toussaint, R. Sedimentary Stylolite Networks and Connectivity in Limestone: Large-Scale Field Observations and Implications for Structure Evolution. *J. Struct. Geol.* **2014**, *63*, 106–123. [CrossRef]

12. Lavenu, A.P.; Lamarche, J.; Texier, L.; Marié, L.; Gauthier, B.D. Background Fractures in Carbonates: Inference on Control of Sedimentary Facies, Diagenesis and Petrophysics on Rock Mechanical Behavior. Example of the Murge Plateau (Southern Italy). *Ital. J. Geosci.* **2015**, *134*, 535–555. [CrossRef]
13. Panza, E.; Agosta, F.; Rustichelli, A.; Zambrano, M.; Tondi, E.; Prosser, G.; Giorgioni, M.; Janiseck, J.M. Fracture Stratigraphy and Fluid Flow Properties of Shallow-Water, Tight Carbonates: The Case Study of the Murge Plateau (Southern Italy). *Mar. Pet. Geol.* **2016**, *73*, 350–370. [CrossRef]
14. Toussaint, R.; Aharonov, E.; Koehn, D.; Gratier, J.-P.; Ebner, M.; Baud, P.; Rolland, A.; Renard, F. Stylolites: A Review. *J. Struct. Geol.* **2018**, *114*, 163–195. [CrossRef]
15. La Bruna, V.; Lamarche, J.; Agosta, F.; Rustichelli, A.; Giuffrida, A.; Salardon, R.; Marié, L. Structural Diagenesis of Shallow Platform Carbonates: Role of Early Embrittlement on Fracture Setting and Distribution, Case Study of Monte Alpi (Southern Apennines, Italy). *J. Struct. Geol.* **2020**, *131*, 103940. [CrossRef]
16. Beaudoin, N.; Gasparrini, M.; David, M.-E.; Lacombe, O.; Koehn, D. Bedding-Parallel Stylolites as a Tool to Unravel Maximum Burial Depth in Sedimentary Basins: Application to Middle Jurassic Carbonate Reservoirs in the Paris Basin, France. *GSA Bull.* **2019**, *131*, 1239–1254. [CrossRef]
17. Beaudoin, N.; Lacombe, O.; Koehn, D.; David, M.-E.; Farrell, N.; Healy, D. Vertical Stress History and Paleoburial in Foreland Basins Unravelled by Stylolite Roughness Paleopiezometry: Insights from Bedding-Parallel Stylolites in the Bighorn Basin, Wyoming, USA. *J. Struct. Geol.* **2020**, *136*, 104061. [CrossRef]
18. Araújo, R.E.; La Bruna, V.; Rustichelli, A.; Bezerra, F.H.; Xavier, M.M.; Audra, P.; Barbosa, J.A.; Antonino, A.C. Structural and Sedimentary Discontinuities Control the Generation of Karst Dissolution Cavities in a Carbonate Sequence, Potiguar Basin, Brazil. *Mar. Pet. Geol.* **2021**, *123*, 104753. [CrossRef]
19. Manniello, C.; Abdallah, I.B.; Prosser, G.; Agosta, F. Pressure Solution-Assisted Diagenesis and Thrusting-Related Deformation of Mesozoic Platform Carbonates. *J. Struct. Geol.* **2023**, *173*, 104906. [CrossRef]
20. Heap, M.J.; Baud, P.; Reuschlé, T.; Meredith, P.G. Stylolites in Limestones: Barriers to Fluid Flow? *Geology* **2014**, *42*, 51–54. [CrossRef]
21. Heap, M.; Reuschlé, T.; Baud, P.; Renard, F.; Iezzi, G. The Permeability of Stylolite-Bearing Limestone. *J. Struct. Geol.* **2018**, *116*, 81–93. [CrossRef]
22. Koehn, D.; Rood, M.P.; Beaudoin, N.; Chung, P.; Bons, P.D.; Gomez-Rivas, E. A New Stylolite Classification Scheme to Estimate Compaction and Local Permeability Variations. *Sediment. Geol.* **2016**, *346*, 60–71. [CrossRef]
23. Humphrey, E.; Gomez-Rivas, E.; Koehn, D.; Bons, P.D.; Neilson, J.; Martín-Martín, J.D.; Schoenherr, J. Stylolite-Controlled Diagenesis of a Mudstone Carbonate Reservoir: A Case Study from the Zechstein_2_Carbonate (Central European Basin, NW Germany). *Mar. Pet. Geol.* **2019**, *109*, 88–107. [CrossRef]
24. Baines, S.J.; Worden, R.H. The Long-Term Fate of CO_2 in the Subsurface: Natural Analogues for CO_2 Storage. *Geol. Soc. Lond. Spec. Publ.* **2004**, *233*, 59–85. [CrossRef]
25. Shedid, S.A.; Salem, A.M. Experimental Investigations of CO_2 Solubility and Variations in Petrophysical Properties Due to CO_2 Storage in Carbonate Reservoir Rocks. In Proceedings of the North Africa Technical Conference and Exhibition, Cairo, Egypt, 15–17 April 2013; OnePetro: Richardson, TX, USA, 2013.
26. Cello, G.; Gambini, R.; Mazzoli, S.; Read, A.; Tondi, E.; Zucconi, V. Fault Zone Characteristics and Scaling Properties of the Val d'Agri Fault System (Southern Apennines, Italy). *J. Geodyn.* **2000**, *29*, 293–307. [CrossRef]
27. Maschio, L.; Ferranti, L.; Burrato, P. Active Extension in Val d'Agri Area, Southern Apennines, Italy: Implications for the Geometry of the Seismogenic Belt. *Geophys. J. Int.* **2005**, *162*, 591–609. [CrossRef]
28. Patacca, E.; Scandone, P. Geology of the Southern Apennines. *Boll. Della Soc. Geol. Ital.* **2007**, *7*, 75–119.
29. Palladino, G.; Prosser, G.; Olita, F.; Avagliano, D.; Dello Iacovo, B.; Giano, S.I.; Bentivenga, M.; Agosta, F.; Grimaldi, S. Reconstruction of the Structural Setting of the North-Eastern Side of the High Agri Valley (Southern Apennines, Italy) Based on Detailed Field Mapping. *J. Maps* **2023**, *19*, 2257729. [CrossRef]
30. Manniello, C.; Agosta, F.; Todaro, S.; Cavalcante, F.; Prosser, G. Fracture Stratigraphy of Mesozoic Platform Carbonates, Agri Valley, Southern Italy. *Geol. Mag.* **2022**, *159*, 1874–1896. [CrossRef]
31. Abdallah, I.B.; Manniello, C.; Prosser, G.; Agosta, F. Multiscale Structural Analyses of Mesozoic Shallow-Water Carbonates, Viggiano Mt., Southern Italy. *J. Struct. Geol.* **2023**, *176*, 104978. [CrossRef]
32. Vezzani, L.; Festa, A.; Ghisetti, F.C. *Geology and Tectonic Evolution of the Central-Southern Apennines, Italy*; Geological Society of America: Boulder, CO, USA, 2010; Volume 469, ISBN 0-8137-2469-4.
33. Shiner, P.; Beccacini, A.; Mazzoli, S. Thin-Skinned versus Thick-Skinned Structural Models for Apulian Carbonate Reservoirs: Constraints from the Val d'Agri Fields, S Apennines, Italy. *Mar. Pet. Geol.* **2004**, *21*, 805–827. [CrossRef]
34. Piedilato, S.; Prosser, G. Thrust Sequences and Evolution of the External Sector of a Fold and Thrust Belt: An Example from the Southern Apennines (Italy). *J. Geodyn.* **2005**, *39*, 386–402. [CrossRef]
35. Noguera, A.M.; Rea, G. Deep Structure of the Campanian–Lucanian Arc (Southern Apennine, Italy). *Tectonophysics* **2000**, *324*, 239–265. [CrossRef]
36. Patacca, E.; Scandone, P.; Bellatalla, M.; Perilli, N.; Santini, U. The Numidian-Sand Event in the Southern Apennines. *Mem. Sci. Geol. Padova* **1992**, *43*, 297–337.
37. Cello, G.; Mazzoli, S. Apennine Tectonics in Southern Italy: A Review. *J. Geodyn.* **1998**, *27*, 191–211. [CrossRef]

38. Doglioni, C.; Harabaglia, P.; Martinelli, G.; Mongelli, F.; Zito, G. A Geodynamic Model of the Southern Apennines Accretionary Prism. *Terra Nova* **1996**, *8*, 540–547. [CrossRef]
39. Giano, S.I.; Maschio, L.; Alessio, M.; Ferranti, L.; Improta, S.; Schiattarella, M. Radiocarbon Dating of Active Faulting in the Agri High Valley, Southern Italy. *J. Geodyn.* **2000**, *29*, 371–386. [CrossRef]
40. Scrocca, D.; Carminati, E.; Doglioni, C. Deep Structure of the Southern Apennines, Italy: Thin-skinned or Thick-skinned? *Tectonics* **2005**, *24*, TC3005. [CrossRef]
41. Agosta, F.; Aydin, A. Architecture and Deformation Mechanism of a Basin-Bounding Normal Fault in Mesozoic Platform Carbonates, Central Italy. *J. Struct. Geol.* **2006**, *28*, 1445–1467. [CrossRef]
42. Bucci, F.; Novellino, R.; Guglielmi, P.; Prosser, G.; Tavarnelli, E. Geological Map of the Northeastern Sector of the High Agri Valley, Southern Apennines (Basilicata, Italy). *J. Maps* **2012**, *8*, 282–292. [CrossRef]
43. Novellino, R.; Prosser, G.; Spiess, R.; Viti, C.; Agosta, F.; Tavarnelli, E.; Bucci, F. Dynamic Weakening along Incipient Low-Angle Normal Faults in Pelagic Limestones (Southern Apennines, Italy). *J. Geol. Soc.* **2015**, *172*, 283–286. [CrossRef]
44. Ferraro, F.; Koutalonis, I.; Vallianatos, F.; Agosta, F. Application of Non-Extensive Statistical Physics on the Particle Size Distribution in Natural Carbonate Fault Rocks. *Tectonophysics* **2019**, *771*, 228219. [CrossRef]
45. Schettino, A.; Turco, E. Tectonic History of the Western Tethys since the Late Triassic. *GSA Bull.* **2011**, *123*, 89–105. [CrossRef]
46. Lechler, M.; Frijia, G.; Mutti, M.; Palladino, G.; Prosser, G. Stratigraphic Setting of a Segment from the Eastern Margin of the Apennine Platform (Monte Di Viggiano, Southern Apennines). *Rend. Online SGI* **2012**, *21*, 1012.
47. Dunham, R.J. Classification of Carbonate Rocks According to Depositional Textures. In *M 1: Classification of Carbonate Rocks—A Symposium*; AAPG: Tulsa, OK, USA, 1962; AAPG Special Volume, pp. 108–121.
48. Marshall, D.J. *Cathodoluminescence of Geological Materials*; Unwin Hyman Ltd.: London, UK, 1988; p. 146. ISBN 004 5520267.
49. Chiocchini, M.; Mancinelli, A. Microbiostratigrafia Del Mesozoico in Facies Di Piattaforma Carbonatica Dei Monti Aurunci (Lazio Meridionale). *Studi Geol. Camerti* **1977**, *3*, 109–153.
50. Chiocchini, M.; Farinacci, A.; Mancinelli, A.; Molinari, V.; Potetti, M. Biostratigrafia a Foraminiferi, Dasicladali e Calpionelle Delle Successioni Carbonatiche Mesozoiche Dell'Appennino Centrale (Italia). *Studi Geol. Camerti* **1994**, *special volume part A*, 9–128.
51. BouDagher-Fadel, M.K.; Bosence, D.W. Early Jurassic Benthic Foraminiferal Diversification and Biozones in Shallow-Marine Carbonates of Western Tethys. *Senckenberg. Lethaea* **2007**, *87*, 1–39. [CrossRef]
52. Preto, N.; Breda, A.; Dal Corso, J.; Franceschi, M.; Rocca, F.; Spada, C.; Roghi, G. The Loppio Oolitic Limestone (Early Jurassic, Southern Alps): A Prograding Oolitic Body with High Original Porosity Originated by a Carbonate Platform Crisis and Recovery. *Mar. Pet. Geol.* **2017**, *79*, 394–411. [CrossRef]
53. Trecalli, A.; Spangenberg, J.; Adatte, T.; Föllmi, K.B.; Parente, M. Carbonate Platform Evidence of Ocean Acidification at the Onset of the Early Toarcian Oceanic Anoxic Event. *Earth Planet. Sci. Lett.* **2012**, *357–358*, 214–225. [CrossRef]
54. Barattolo, F.; Romano, R. Shallow Carbonate Platform Bioevents during the Upper Triassic-Lower Jurassic: An Evolutive Interpretation. *Ital. J. Geosci.* **2005**, *124*, 123–142.
55. Di Stefano, P.; Ruberti, D. Cenomanian Rudist-Dominated Shelf-Margin Limestones from the Panormide Carbonate Platform (Sicily, Italy): Facies Analysis and Sequence Stratigraphy. *Facies* **2000**, *42*, 133–160. [CrossRef]
56. Andrews, L.M.; Railsback, L.B. Controls on Stylolite Development: Morphologic, Lithologic, and Temporal Evidence from Bedding-Parallel and Transverse Stylolites from the US Appalachians. *J. Geol.* **1997**, *105*, 59–73. [CrossRef]
57. Oelkers, E.H.; Bjørkum, P.A.; Walderhaug, O.; Nadeau, P.H.; Murphy, W.M. Making Diagenesis Obey Thermodynamics and Kinetics: The Case of Quartz Cementation in Sandstones from Offshore Mid-Norway. *Appl. Geochem.* **2000**, *15*, 295–309. [CrossRef]
58. Renard, F.; Dysthe, D.; Feder, J.; Bjørlykke, K.; Jamtveit, B. Enhanced Pressure Solution Creep Rates Induced by Clay Particles: Experimental Evidence in Salt Aggregates. *Geophys. Res. Lett.* **2001**, *28*, 1295–1298. [CrossRef]
59. Sheldon, H.A.; Wheeler, J.; Worden, R.H.; Cheadle, M.J. An Analysis of the Roles of Stress, Temperature, and pH in Chemical Compaction of Sandstones. *J. Sediment. Res.* **2003**, *73*, 64–71. [CrossRef]
60. Kristiansen, K.; Valtiner, M.; Greene, G.W.; Boles, J.R.; Israelachvili, J.N. Pressure Solution–The Importance of the Electrochemical Surface Potentials. *Geochim. Cosmochim. Acta* **2011**, *75*, 6882–6892. [CrossRef]
61. Aharonov, E.; Katsman, R. Interaction between Pressure Solution and Clays in Stylolite Development: Insights from Modeling. *Am. J. Sci.* **2009**, *309*, 607–632. [CrossRef]
62. Koehn, D.; Renard, F.; Toussaint, R.; Passchier, C. Growth of Stylolite Teeth Patterns Depending on Normal Stress and Finite Compaction. *Earth Planet. Sci. Lett.* **2007**, *257*, 582–595. [CrossRef]
63. Ebner, M.; Koehn, D.; Toussaint, R.; Renard, F.; Schmittbuhl, J. Stress Sensitivity of Stylolite Morphology. *Earth Planet. Sci. Lett.* **2009**, *277*, 394–398. [CrossRef]
64. Park, W.C.; Schot, E.H. Stylolites; Their Nature and Origin. *J. Sediment. Res.* **1968**, *38*, 175–191.

65. Ebner, M.; Toussaint, R.; Schmittbuhl, J.; Koehn, D.; Bons, P. Anisotropic Scaling of Tectonic Stylolites: A Fossilized Signature of the Stress Field? *J. Geophys. Res.* **2010**, *115*, B06403. [CrossRef]
66. Bruns, B.; Di Primio, R.; Berner, U.; Littke, R. Petroleum system evolution in the inverted Lower Saxony Basin, northwest Germany: A 3D basin modeling study. *Geofluids* **2013**, *13*, 246–271. [CrossRef]

Disclaimer/Publisher's Note: The statements, opinions and data contained in all publications are solely those of the individual author(s) and contributor(s) and not of MDPI and/or the editor(s). MDPI and/or the editor(s) disclaim responsibility for any injury to people or property resulting from any ideas, methods, instructions or products referred to in the content.